Counter-current arrangement of microfluidic liquid-liquid droplet flow contactors

Abstract: The objective of microfluidic droplet flow is the control and manipulation of fluids on the sub-mm scale. This article describes the microfluidic droplet flow in a liquid-liquid contacting unit utilizing microchannels and millichannels and their counter-current arrangement. A contacting module consists of a droplet generator, a channel to enable an intensified mass transfer between two fluids and a liquid-liquid separation device. Experiments were performed with deionized water as a continuous phase and various organic solvents as a dispersed phase. The organic droplets are generated by direct coflowing injection through a needle located in the center of the microchannel. Droplet generation and flow patterns were optically investigated in straight and winding channels. The adjacent separation unit continuously splits the organic, dispersed phase. The combined effects of gravity, wetting characteristics of the wall material and capillary forces nearly completely separate the two fluids over a wide range of flow rates. Based on the mixer-settler system, a microfluidic extraction unit is proposed that enables a multistage counter-current arrangement.

Keywords: counter-current arrangement; downstream processing; microfluidic droplet flow; mixer-settler.

*Corresponding author: Alexander Holbach, TU Dortmund, Biochemical and Chemical Engineering, Equipment Design, Emil-Figge-Straße 68, 44227 Dortmund, Germany, e-mail: alexander.holbach@bci.tu-dortmund.de
Norbert Kockmann: TU Dortmund, Biochemical and Chemical Engineering, Equipment Design, Emil-Figge-Straße 68, 44227 Dortmund, Germany

1 Introduction

One major goal of the chemical and biochemical industry in recent decades has been the intensification of chemical processes. The precise control of the unit operations with high heat and mass transfer rates leads to less energy consumption, less chemical waste and less unwanted byproducts [1]. The miniaturization of devices is one important step to optimize the transport processes.

The short diffusion length and the large specific surface inside the microstructured equipment allow for an implementation of transport-limited processes [2]. Important developments for single- and two-phase systems are summarized by Hessel et al. [3], Kockmann [4] and Kashid et al. [5].

The applications of liquid-liquid processes in microchannels are the same as in classical equipment, but the major benefit is enhanced heat and mass transport. These advantages allow for rapid equilibration times, a low fluid hold up and flexible and safer processes. Currently, many articles describe the benefits of microstructured devices for liquid-liquid separation technologies for co-current [5, 6] and constructions of counter-current flow regimes [7, 8]. A typical technique for counter-current flow in the field of microfluidics is the two-phase flow in one single microchannel. Nevertheless, additional forces are necessary to stabilize the free interface between the two fluids. This can be the capillary force employed in sieve structures [8, 9] and membranes [10] or the interfacial force stabilized by wettability effects of the wall [11]. The second possibility is an indirect counter-current flow such as in a classical mixer-settler arrangement. The liquidliquid flow inside the channel is co-current, whereas the arrangement of the contacting modules is counter-current [12]. The advantage of this setup is a higher hydrodynamic flexibility. The disadvantage is the necessity of one additional pump between each mixer-settler unit to implement the counter-current arrangement. This article deals with the second possibility, a counter-current arrangement realized as a mixer-settler system.

In microstructured devices, generally four coflowing flow regimes can be observed: the parallel flow, the regular droplet flow, the slug flow and the irregular dispersed flow (see Figure 1). The laminar flow produces a parabolic velocity profile inside the channel, which is locally influenced by the liquid-liquid surface of the different flow patterns. To predict the regime, it is important to consider several system parameters and fluid properties, such as channel geometry, velocity, volume ratio, viscosity and density of both phases, surface tension and the wettability to the wall material. Different flow patterns produce different mass transfer rates, pressure drops and phase-separation behavior.

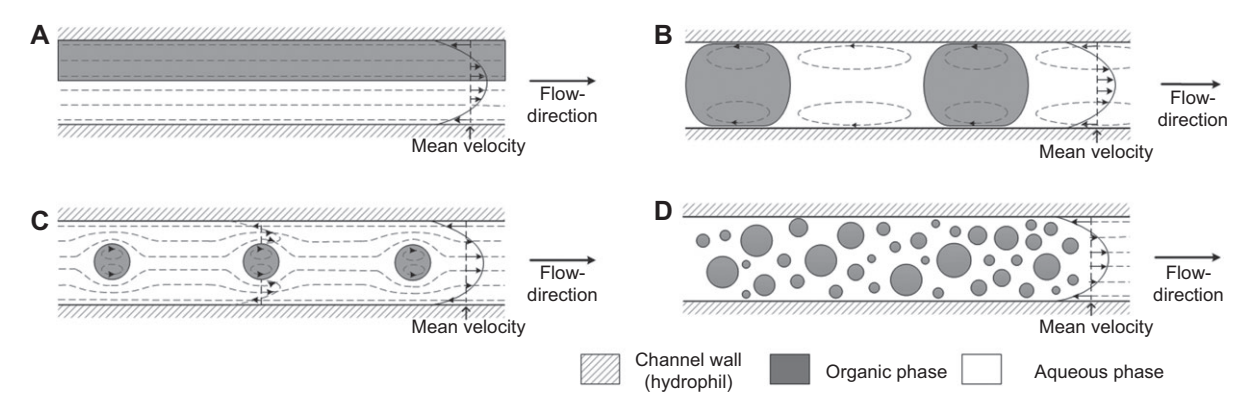


Figure 1 Liquid-liquid flow patterns in microchannels with streamlines and relative velocity profile.

(A) Parallel flow; (B) slug flow; (C) regular droplet flow; (D) irregular dispersed flow. The annular flow is not shown here.

Regular flow patterns are easier to separate because of their well-controlled physical and rheological properties. This has already been shown for the slug flow [13, 14]. The phase separation of irregular dispersed flows takes much more time because of their wide drop-size distribution. However, higher specific surfaces and therefore higher mass transport rates can usually be reached with these irregular flow regimes. Aoki et al. [15] compared the mass transfer and the phase-separation times of the irregular dispersed and slug flows. The results showed that the mass transfer times of the irregular dispersed flow are higher than the slug flow, but the separation of the two fluids takes much longer.

This paper describes the characteristics of microfluidic devices or modules for droplet generation, two-phase flow in microstructured channels and successful phase separation at the channel outlet. After a short description of experimental methods, the droplet generation in the channel is characterized by the channel flow and phase separation of the liquid-liquid flow. The flow regime, the specific surface and the counter-current arrangement with a stack setup were investigated. Inside the contacting module of the mixer-settler, a regular droplet flow was realized and characterized. The regular droplet flow regime has the advantage of a large specific surface and, thus, good mass transfer. Additionally, a regular droplet size allows for well-controlled separation in a short time.

2 Materials and methods

The experiments were performed with a droplet-generation setup made of stainless steel, an adjacent glass plate with microchannel and a separation device made of stainless steel for the aqueous outlet and of PEEK (polyether ether ketone) for the organic outlet. The droplet generation and separation devices were home designed and fabricated in our workshop. The tightness between the steel and glass was secured by a PTFE (polytetrafluoroethylene) seal. The PEEK element in the separation device was pressed into the stainless steel separation device. The stainless steel sieve (pore size, 400 μm) was soldered onto the slanted end of a hollow ferrule and introduced into the separation device. The channel in the glass plate, from the Little Things Factory (LTF, Elsoff, Germany) had a length of 2 m and an internal volume of 1.6 ml. The entire device was kept at a constant temperature. The system configuration is shown schematically in Figure 2. A scheme of the experimental setup is shown in Figure 3.

For droplet generation, the organic dispersed phase was pumped through a stainless steel needle (B. Braun, Melsungen, Germany) and formed droplets or a jet, which also broke up into droplets. The needle had an inner diameter of 200 µm and was located in a 1000-µm-wide channel with a nearly circular cross section of the glass plate. The organic dispersed phase was pumped with a continuously operating syringe pump (MR Q, MMT, Siegen, Germany) or a peristaltic pump (Reglo, Ismatec, Wertheim-Mondfeld, Germany). The aqueous continuous phase was pumped with a low pulsation rotating gear pump (mzr-7255, HNP Mikrosysteme, Parchim, Germany). The optical studies were performed with a microscope (ADL 601P, Bresser) and a digital camera (D 7000, Nikon). The pressure was measured in the continuous phase at the inlet and outlet with conventional pressure sensors (A-10, Wika, Klingberg am Main, Germany).

The investigation of the liquid-liquid flow was performed with n-nonane as the organic phase (Merck >99%) and deionized water as the aqueous phase. The temperature was kept constant at 20°C. The flow patterns were compared with those of n-heptane and n-undecane (Merck >99%). For better flow pattern characterization, the organic phase was

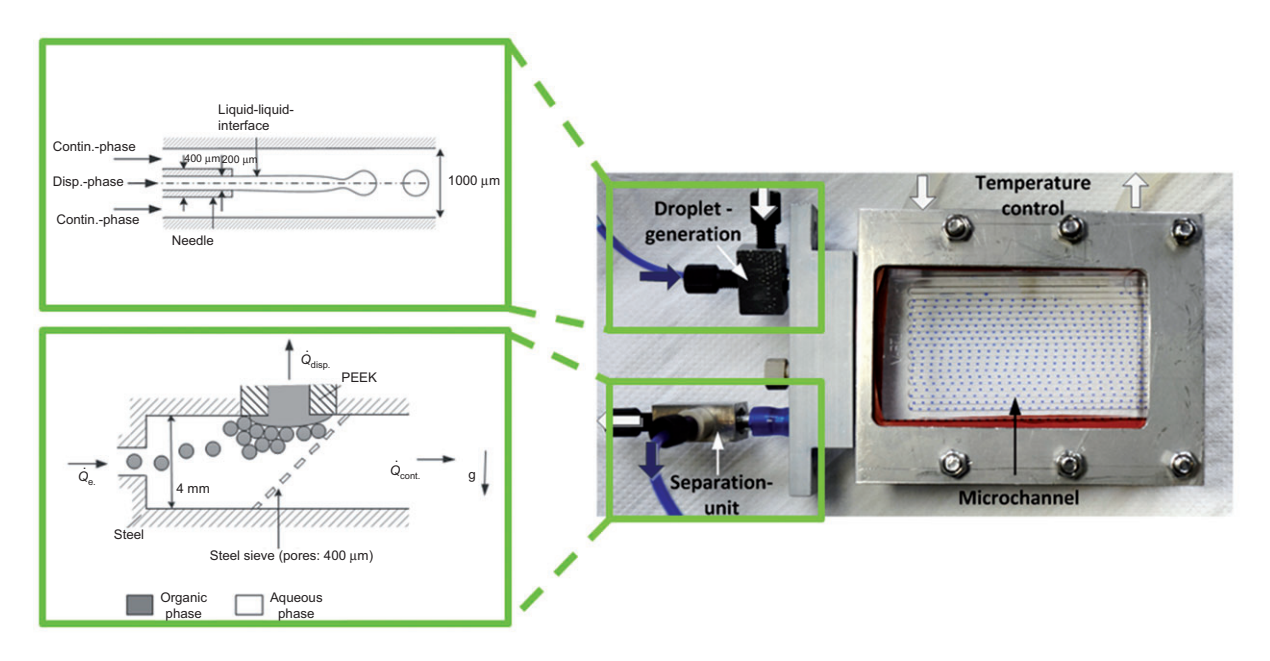


Figure 2 Picture of the experimental setup of the contacting module.

Left side, connectors with droplet generation and phase separation; right side, temperature controlled glass plate with microchannel.

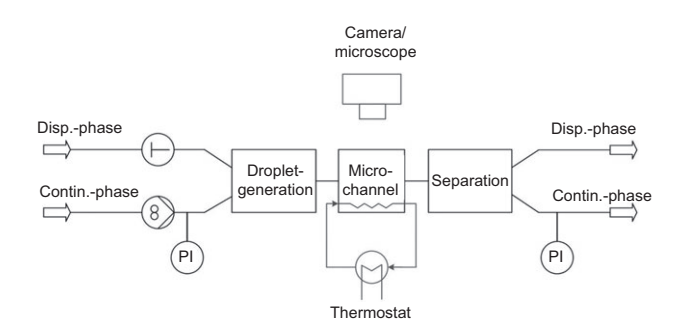


Figure 3 Flow scheme of the experimental configuration of one contacting module.

dyed with Sudan Blue (Sigma Aldrich). The mass transfer investigations were performed with 0.5 M acetic acid (Merck, >99%) in n-nonane and 0.05 M sodium hydroxide (Merck, >97%) in deionized water. Bromothymol blue (AppliChem) was used as a color indicator for pH-values.

3 Hydrodynamics and mass transfer of the regular droplet flow

3.1 Fundamentals for droplet generation and flow

The first contact of the two immiscible fluids happens during droplet generation at the needle tip. To describe

the hydrodynamic effects, characteristic dimensionless numbers are defined at this place. The capillary number *Ca* compares the viscous to surface forces, the Weber number, *We*, is the ratio of inertial to surface forces, and the Eötvös number, *Eö*, compares gravity to the surface force:

$$Ca = \frac{\mu v}{\sigma}, We = \frac{\rho v^2 d_d}{\sigma}, E\ddot{o} = \frac{\Delta \rho g d_d^2}{\sigma}, Re = \frac{We}{Ca} = \frac{\rho v d_d}{\mu}.$$
 (1)

The Reynolds number, Re, is the ratio of the Weber number, We, and the capillary number, Ca, and describes the flow regime within the channel. The diameter, d_a , is the mean diameter of the droplets, μ is the characteristic dynamic viscosity of the dispersed phase and v is the velocity of the organic phase at the needle tip. Finally, the surface tension, the density difference between the two phases is given, respectively, by σ and $\Delta \rho$. The dimensionless numbers for the experiments are shown in Table 1. In the investigated range, the surface forces are dominating in comparison to the viscous and gravitational forces (low Ca and $E\ddot{o}$ numbers). For high flow velocities, the inertial forces have to be considered, along with the We and Re numbers.

Table 1 Range of dimensionless numbers for the organic, dispersed phase (0.05–1.6 m/s n-nonane velocity) during the droplet generation at the needle tip, 20°C.

Re	We	Са	Eö
11-400	1×10 ⁻² -10	9×10 ⁻⁴ -2.5×10 ⁻²	1.2×10 ⁻² -3.3×10 ⁻²

The dimensionless numbers describe only the liquidliquid behavior. However, the stability of the flow inside the channel is strongly influenced by the contact between the fluids and the channel wall. Experiments have shown that it is only possible to keep regular droplet or slug flow if the continuous phase wets the wall material, i.e., hydrophilic walls for continuous aqueous phases or hydrophobic walls for continuous organic phases. For non-suitable materials, the phase inversion in the channel will change the flow patterns.

3.2 Droplet generation process

The equipment uses co-current modules for the countercurrent arrangement. The droplets in each module are generated by a centered needle in a glass channel. Both phases come into contact at the co-current injection of the organic, dispersed phase into the aqueous, continuous phase. Figure 4 shows a sketch of the arrangement and the resulting images of the droplet generation. Depending on the flow velocity of the organic phase, two different types of droplet generation are observed in the interesting range. At low velocities of the organic phase and low Ca numbers, the droplets are directly generated at the needle tip. During this dripping mode, the droplets are growing at the needle tip until the shear forces between the continuous and dispersed phases are high enough to detach the droplets (see Figure 4B). The production of monodisperse droplets with small diameters is possible.

At higher flow velocities, the organic phase produces a liquid jet in the channel. During this second mode,

the liquid jet breaks up into small droplets as a result of the Rayleigh-Plateau instability (see Figure 4C). General investigations of dripping and jetting are given by Barrero and Loscertales [16]. The results could indicate that the control of the droplet generation is so accurate that it is possible to produce monodisperse microparticles and multi-emulsions with this technique.

The influence of the $\it Ca$ number on droplet generation in microchannels is given in Figure 5, indicating the effect of the velocity of the organic phase. The dripping mode produces larger droplets, with diameters, $\it d_d$, of approximately 700 μ m. The error of the droplet diameter is below 5%. The velocity of the continuous phase has a large influence on droplet size during the dripping mode. Higher flow velocity, $\it u_{cont.}$, leads to larger shear forces and smaller droplets. With increasing $\it Ca$ numbers and increasing viscous forces, droplet generation changes from dripping to jetting mode.

The jetting mode produces smaller droplets with diameters of approximately 400 μm . A comparison of the droplet diameter for different velocities of the continuous phase shows that the droplet generation at the Rayleigh Plateau instability is more independent from the shear forces. Thus, the droplet size for different velocities, $u_{cont.}$, is nearly the same in the investigated range.

3.3 Classification of flow patterns in the glass channel

Different flow regimes in the microchannel can be observed depending on the volumetric flow rates of the

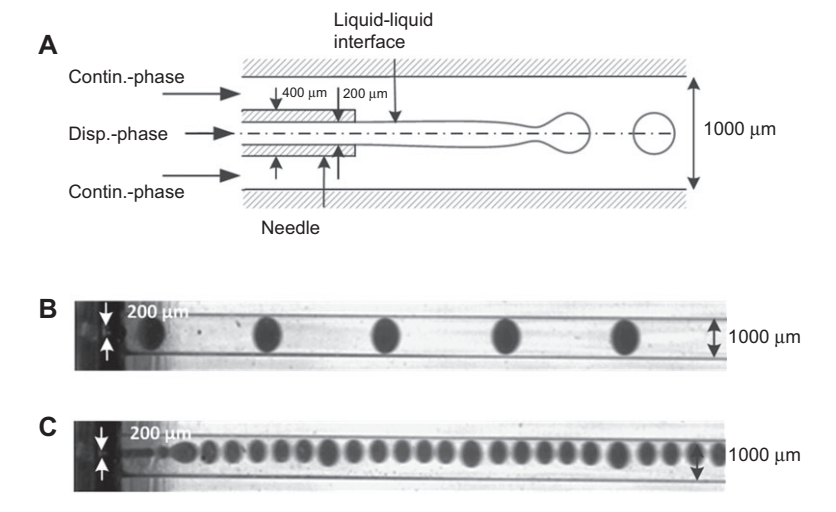


Figure 4 Droplet generation with coflowing injection in microchannels.

(A) Sketch of the injection region; (B) dripping mode (0.15 m/s continuous phase and 0.53 m/s dispersed phase, n-nonane); (C) jetting mode (0.15 m/s continuous phase and 1.06 m/s dispersed phase, n-nonane).

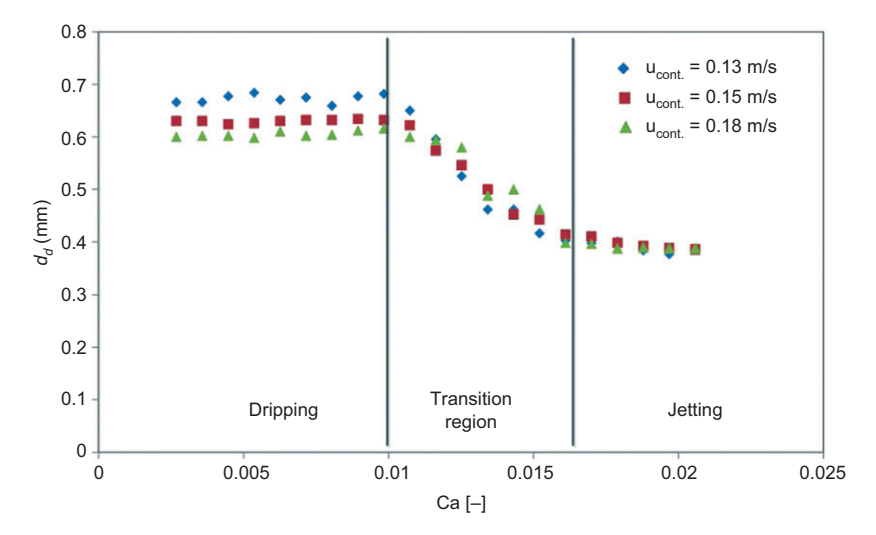


Figure 5 Diameter of n-nonane droplets based on the Ca number and constant continuous velocities, $u_{cont.}$ (error \leq 5%). The Ca number and velocities are defined at the injection region for the continuous and dispersed inlets, respectively.

immiscible fluids. In the flow pattern maps in Figure 6, the flow regimes for n-heptane, n-nonane and n-undecane are indicated. The flow pattern for n-nonane includes images of the resulting liquid-liquid flow. As

can be observed, the regular droplet flow is possible with all three organic phases. N-nonane and n-undecane show similar behavior, i.e., dripping mode with smaller organic volume flow rates and jetting mode

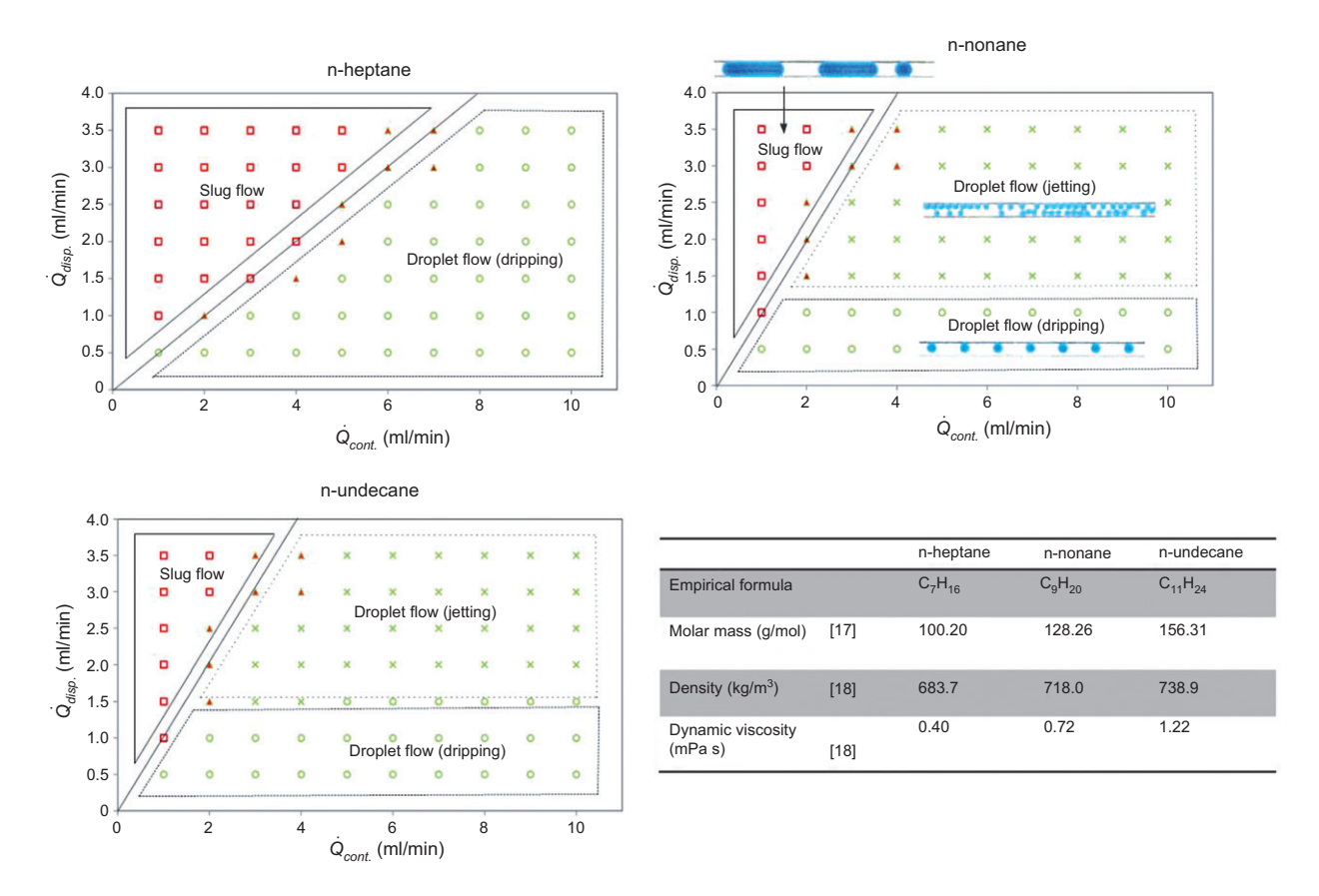


Figure 6 Flow pattern map and operation window in the microchannel as a function of the volume flow rate of the continuous phase (water) and the organic, dispersed phase (continuous phase 0.13 m/s ≙ 5 ml/min). The table gives the properties of the three organic phases.

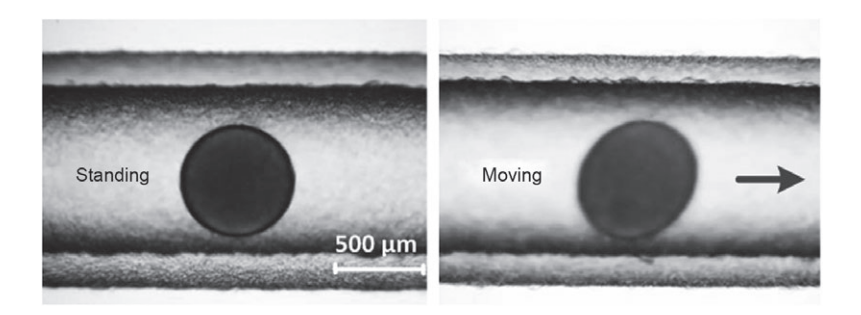


Figure 7 Picture of a droplet (n-nonane) in the microchannel. Left, droplet at rest; right, moving, off-centric droplet with a mean flow velocity in the channel of 0.056 m/s ≜ 3.4 ml/min.

with higher organic volume flow rates. As mentioned in Section 3.1, the transition from dripping to jetting is mainly influenced by the Ca number, or the volume flow rate of the injected, dispersed phase. This is indicated by the horizontal transition region between dripping and jetting of the dispersed volume flow rate Q_{disp} . With n-heptane, no jetting was observed. The production of a symmetric, liquid jet in the channel is not possible; only the dripping mode can be observed because the viscous forces are too small. The droplet flow, which is produced in both cases from dripping and jetting, can be obtained over the entire channel length of 2 m. Less coalescence was observed in the continuous flow of the aqueous phase due to the suitable, hydrophilic wall material. For lower continuous flow rates than dispersed flow rates, the droplet flow in the channel disappeared and slug flow was observed. As an effect of the lower continuous volume flow rate and wall influence, the phase inversion forms an irregular slug flow. To maintain regular droplet flow in microchannels, it is necessary to have larger continuous flow rates than dispersed flow rates.

Influences on the droplet flow of the inertial forces can be observed by a comparison between a moving droplet and a droplet at rest. The resting droplet forms a perfect sphere, whereas the moving droplet is deformed (see Figure 7). This effect is more significant with increasing droplet diameters and increasing flow velocities. The inertial forces deform the droplets depending on the parabolic velocity profile inside the channel.

The droplet deformation is relatively small compared to its diameter and can be neglected for the calculation of the specific surface-to-volume-ratio (S/V). S/V indicates the effective interface between the two fluids for spherical droplets:

$$\frac{S}{V} = \frac{6}{d_d} \frac{\dot{Q}_{dis.}}{\dot{Q}_{dis.} + \dot{Q}_{cont.}} \tag{2}$$

Volume, V, is based on the total volume of the continuous and dispersed phases. The droplet diameter, d_{x} is an average of 10 droplets.

Changes in the diameter of the droplets and flow rates have direct influence on the specific interface. Figure 8 shows the resulting S/V for three different flow rates of 5, 6, and 7 ml/min of the continuous phase, n-nonane over the flow rate of the dispersed phase. High flow rates of the dispersed phase and low flow rates of the continuous phase lead to small droplet diameters and large S/V-ratios, up to 5000 m²/m³. The comparison with common contacting modules such as agitated contactors $(S/V=32-311 \text{ m}^2/\text{m}^3)$ [19], extraction columns with random packing $(S/V=80-450 \text{ m}^2/\text{m}^3)$ [20] and microfluidic slug flow contactors ($S/V=830-3200 \text{ m}^2/\text{m}^3$) [21] are included in the diagram to compare the different contactors.

3.4 Mass transfer of the regular droplet flow

To characterize the mass transfer of the regular droplet flow, a fast neutralization reaction is implemented.

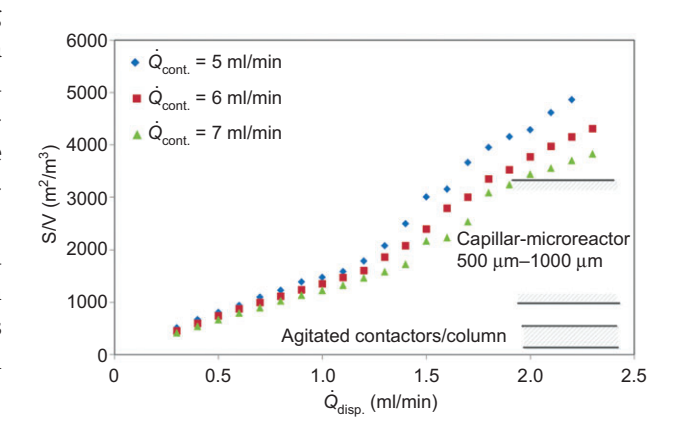


Figure 8 Effective interfacial area between the liquids (n-nonane/water) in the 1000-µm channel in comparison to other micro and conventional contactors.

$$CH_3COOH_{org.} + NaOH_{adj.} \rightarrow CH_3COO \cdot Na_{adj.}^+ + H_2O$$
 (3)

The reaction is a tool for characterizing the transport process within the liquid-liquid system. Acetic acid diffuses from the organic phase to the aqueous phase and reacts there with sodium hydroxide to sodium acetate and water. The concentration of the acid is 0.5 M in n-nonane; the base has a concentration of 0.05 M in deionized water. As a response to the reaction, the pH value in the aqueous phase changes and is indicated by bromothymol blue. The color changes from blue-basic to yellow-acidic at a pH value of 7. Different colors indicate concentration profiles, and thus the mass transport in the continuous phase. Dessimoz et al. [6] employed trichloro acetic acid to determine the mass transfer in slug and parallel flow regimes. Further liquid-liquid test reactions to characterize twophase mixing in microchannels have been summarized by Kockmann and Roberge [22].

Due to the instantaneous reaction of the neutralization, the whole process is mass transfer limited. The color change is directly influenced by the hydrodynamics of the microfluidic system. The fluid flow in two different microchannels/millichannels is shown in Figure 9. The first straight channel is 1000 µm wide; the second winding channel has a diameter between 1000 and 2000 µm. Both experiments were conducted with the same acid and base concentrations and the same flow rates of 1 ml/min for the organic phase and 6 ml/min for the aqueous phase. The fluid dynamics of the straight channel is determined by the laminar flow profile of the continuous phase. Because the flow velocity is higher in the middle of the straight channel than at the wall, a yellow string is formed between the droplets. In contrast, the fluid dynamics in the winding channel is dominated by an additional crossmixing in the laminar flow. The channel structure disturbs the symmetry of the laminar flow. The continuous phase is strongly mixed of the channel. The Dean number in the winding channel is between 10 and 150, depending on the flow velocity in the channel. Higher mass transfer rates are observed by shorter channel lengths for complete mixing. Comparable effects were observed for the gas-liquid slug flow [23] and single phase chaotic mixers [24]. More detailed investigations of mass transfer for liquid-liquid parallel and annular flow regimes were studied by Janovic et al. [25]. They measured mass transfer coefficients in 250-um channels in the range of 3-0.5 s⁻¹. These high mass transfer rates should also be used for counter-current applications.

4 Continuous separation of the immiscible fluids

For continuous two-phase processes of co-current modules in counter-current arrangements, an instantaneous and robust phase-separation step is necessary. In this work, the separation is based on combined gravity, capillary and surface forces. To enhance the coalescence, two different materials are used with PEEK for the organic phase, and stainless steel is used for the aqueous phase outlet. The continuous phase wets the stainless steel wall and passes the capillary pores of the sieve to the aqueous outlet, whereas the dispersed phase moves up, wets the PEEK wall and flows through the organic outlet (see Figure 10).

The expansion to the mm scale slows down the flow velocity and allows for good phase separation as a settler in a reasonable time. With a diameter of 4 mm and a volume of 0.3 ml, the droplets have a residence time between 0.1 and 1 s. The influence of gravity on the microscale and milliscale is small, but in combination with the capillary and surface forces, the separation unit works over a wide range of volume flow rates. To achieve full phase separation in a short residence time, regular, monodisperse droplets are very helpful due to their homogeneous characteristics.

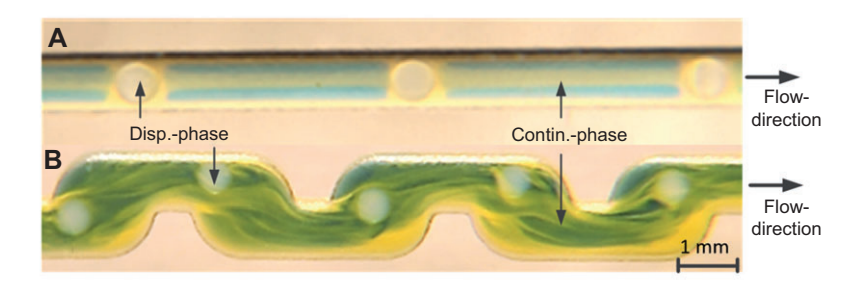


Figure 9 Visualization of the mass transfer with a neutralization reaction (n-nonane/water: 1/6 ml/min). (A) Straight channel; (B) winding channel.

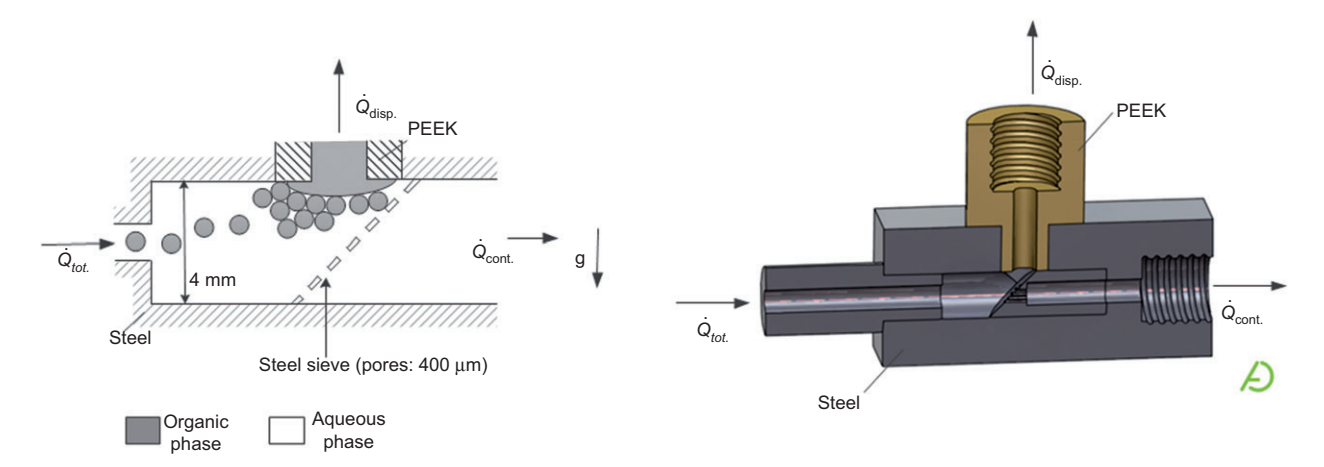


Figure 10 Schematic of the phase-separation area.

The expansion to the milliscale allows an instantaneous phase separation with additional gravity, capillary and surface forces. Left side, scheme of the liquid-liquid phase separation; right side, CAD-sectional view.

During separation, the total volume rates of both fluids must be conserved. The total volume flow, $\dot{Q}_{tot.}$, separates into the dispersed, $\dot{Q}_{disp.}$, and continuous, $\dot{Q}_{cont.}$, flow rates:

$$\dot{Q}_{tot} = \dot{Q}_{dis} + \dot{Q}_{cont} . \tag{4}$$

The volume conservation requires the same pressure drop for the continuous and dispersed outlets [26]. To be independent of the pressure drop, an additional pump for the organic outlet had to be installed. With this arrangement, a nearly complete partitioning of the two phases was possible over the investigated flow rate range. Figure 11 shows the separation of the n-nonane

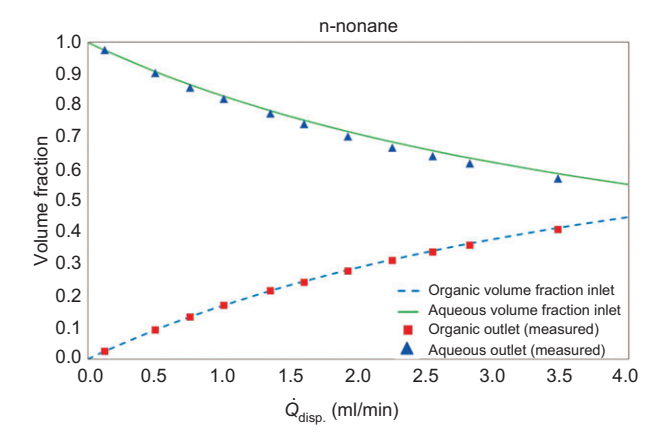


Figure 11 Volume fraction of the separation device. Solid and dashed lines represent volume fractions of water and n-nonane, respectively, at the inlet. Data points are the corresponding measured volume flow rates based on the collected volume at the respective outlet. The aqueous flow rate is kept constant at 5 ml/min.

droplet flow. The inlet volume fractions of the two phases (solid and dashed lines) are compared with measured volume flow rates at the organic and aqueous outlets, respectively, based on the total volume flow rate (data points). For this experiment, the continuous, aqueous volume flow rate was kept constant at 5 ml/min, whereas the organic, dispersed volume flow rate was varied from 0.1 to 3.5 ml/min. The device shows for this operational window a partitioning of over 98 vol%. For counter-current applications, the phase recovery in the false direction will decrease the efficiency. It disturbs the accurate droplet generation in the following stage and makes the separation more difficult. The recovery in the "false" stage will also decrease the extraction efficiency. Hence, it is important to have a robust phase separation for a counter-current setup.

5 Counter-current arrangement of contacting modules

The counter-current flow arrangement was realized and investigated with a two-stage contacting module. The left side of Figure 12 shows the arrangement of the contacting units together with the pressure profile over the stages. The aqueous continuous phase flows directly from the first to the last stage with one feed pump. The organic, dispersed phase needs one additional pump between every stage to reach the pressure level of the next stage for counter-current flow. This arrangement requires (*n*+1) pumps and one pressure-control valve for the dispersed phase outlet.

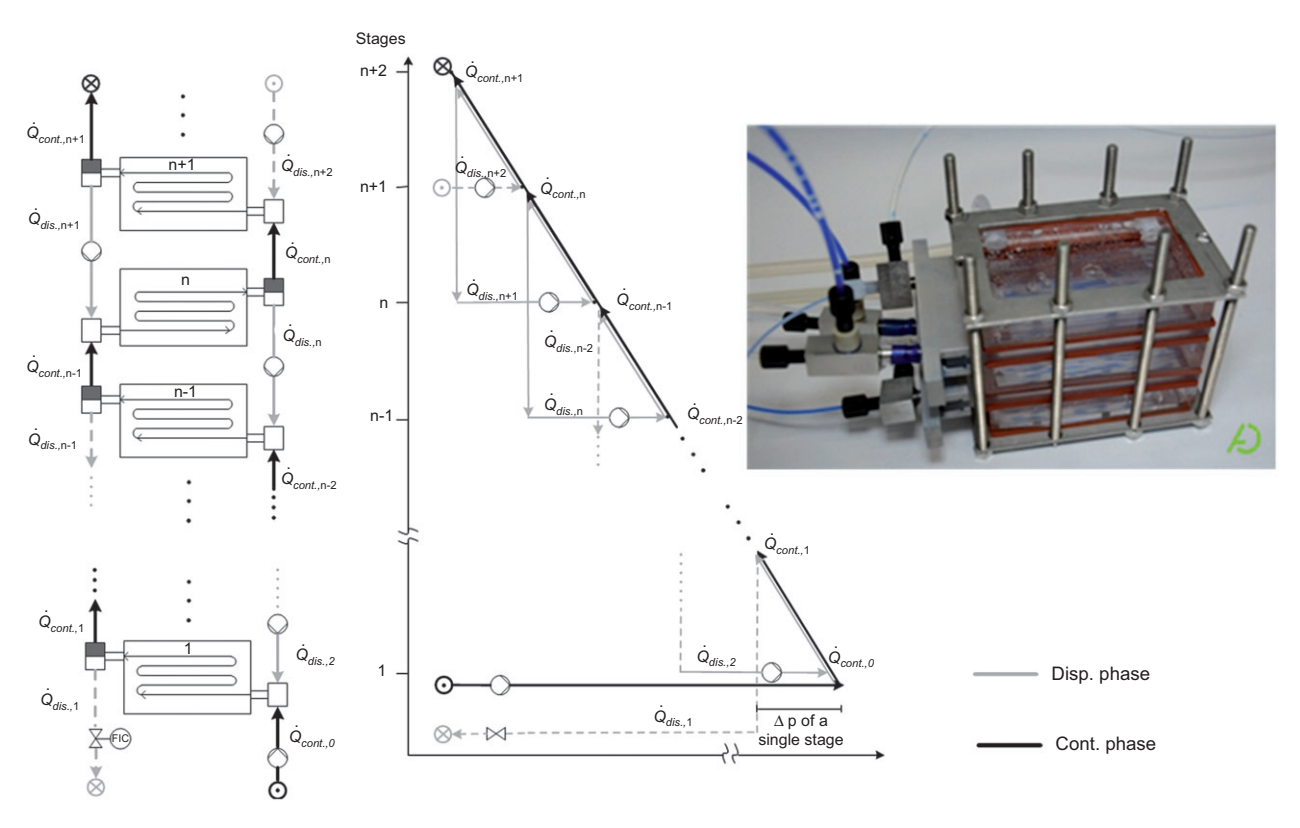


Figure 12 Counter-current arrangement. On the left side, configuration and pressure profile over the stages; on the upper right corner, the experimental stack with droplet generation+separation and two glass plates (channel size: Ø=1000 μm; L=2 m; V=3.8 ml).

The summed-up pressure drop for the continuous phase is the overall pressure drop over N stages. The pressure drop in a single stage consists of the sum of the pressure loss from droplet generation, $\Delta p_{g,i}$, microchannel flow, $\Delta p_{c,i}$, and separation, $\Delta p_{s,i}$:

$$\Delta p = \sum_{i=1}^{N} \left(\Delta p_{g,i} + \Delta p_{c,i} + \Delta p_{s,i} \right) N \text{ stages}$$
 (5)

The pressure drop in the channel is proportional to the velocity and inversely proportional to the square of the channel diameter. The pressure drop can be approximate with a modified Hagen-Poiseuille equation [27].

$$\Delta p_{c,i} = \frac{8\mu_{cont.} \left(\dot{Q}_{cont.} + \dot{Q}_{disp.}\right) L_c}{\pi \left(\frac{d_c}{2}\right)^4}.$$
 (6)

For the operational window of the droplet flow, a pressure drop up to 0.2 bar for one stage was observed. The main pressure drop occurred with 0.18 bar in the channel, with a diameter of 1000 µm, a length of 2 m and flow rates for the aqueous phase of 10 ml/min.

The image in the right side of Figure 11 shows an experimental two-plate stack of a counter-current

arrangement, with droplet generation and separation units. The glass plates with microchannels are stacked within a surrounding temperature bath. The flow rate of the organic phase between the stages is controlled by a four-stage peristaltic pump in this counter-current flow experiment. The pulsation of the pump allows only smaller operational windows than the accurate syringe pump, but it is possible to pump all organic streams with one device. The entire construction is shown in Figure 13 with pump, tubes and flask for the organic and aqueous phases. The inputs of the two stages were placed on the same side to have the shortest connections possible. The setup shows the feasibility of the counter-current arrangement. Droplet generation and phase separation work in this counter-current configuration.

6 Conclusion and outlook

This experimental work shows the possibility of microfluidic droplet flow in microchannels and millichannels for chemical reactions and liquid-liquid extraction. The

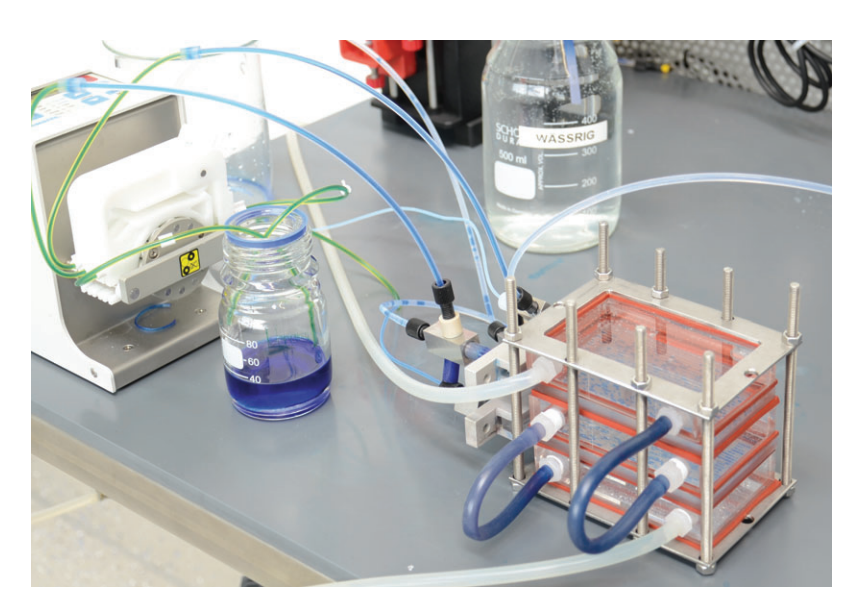


Figure 13 Complete two-stage counter-current setup with pumps, tubes and flask for organic (blue color) and aqueous phases. The tubes for the temperature control fluid are visible at the front side of the stack.

accurate droplet generation with dripping and jetting modes produces well-controlled flow patterns inside the channel. The production of small monodisperse droplets is possible in the jetting mode. The resulting microfluidic flow regime shows higher specific surfaces in comparison with ordinary contactors and microcapillary contactors. With winding channels, it is possible to add additional cross-mixing and disturb the symmetry of the flow with increased mass transfer. The following phase separation after the channel operates continuously with a small hold-up over a wide range of flow rates. The entire setup, with droplet generation, residence time and mixing channel and separation, allows for good and modular application for co-current and counter-current liquid-liquid processes. The counter-current arrangement needs additional pumps for the dispersed phase to maintain the pressure profile. The experimental verification of a two-plate counter-current cascade demonstrates the proof of principle. However, there are still major challenges for the counter-current arrangement of droplet flow contactors.

For the realization of the counter-current extraction unit, the resulting mass transfer has to be determined in future experiments. To predict possible extraction systems, it is necessary to understand the different influences of channel geometry, physical and chemical properties of the organic phase, and phase separation. For more than two counter-current stages, precise pumps are necessary. This is important to yield the regular droplet flow and enable proper phase separation.

Acknowledgements: We would like to express our sincere thanks to Delphine Berset, Prof. Thierry Chappuis and Prof. Ulrich Scholten for constructive discussion within the exchange program between Ecole d'ingénieurs et d'architectes de Fribourg and the TU Dortmund University.

Received January 28, 2013; accepted February 28, 2013

References

- Anastas, PT, Heine, LG, Williamson, TC. Green Engineering, American Engineering Society: Washington, DC, 2000.
- [2] Chasanis P, Kehrmann KM, Kern J, Grünewald M, Kenig EY. Chem. Eng. Process. 2011, 50, 1244–1251.
- [3] Hessel, V, Hardt, S, Löwe, H. *Chemical Micro Process Engineering*, Wiley-Verlag: Weinheim, 2004.
- [4] Kockmann, N. *Transport Phenomena in Micro Process Engineering*, Springer: Berlin, 2007, pp. 3–6.
- [5] Kashid MN, Renken A, Kiwi-Minsker L. Chem. Eng. Sci. 2011, 66, 3876–3897.
- [6] Dessimoz AL, Cavin C, Renken A, Kiwi-Miosker L. Chem. Eng. Sci. 2008, 63, 4025–4044.

- [7] Wojik A, Marr R. Chem. Ing. Tech. 2005, 77, 653-668.
- [8] Chasanis P, Kern J, Grünewald M, Kenig EY. Chem. Ing. Tech. 2010, 82, 215-218.
- [9] Ehrfeld, W, Löwe, H, Hessel, V, Richter, T. In Microreaction Technology IMRET 1, Ehrfeld W, Ed., Springer-Verlag: Berlin, 1997, pp. 72-90.
- [10] TeGrotenhuis, WE, Cameron, RJ, Viswanathan, VV. Proceedings of 3rd International Conference on Microreaction Technology, 1991, pp. 541-549.
- [11] Robins, I, Shaw, J, Miller, B, Turner, C, Harper, M. Proceedings of 1st International Conference on Microreaction Technology, IMRET 1, 1997, pp. 35-46.
- [12] Agar, DW. Extraction in μ -Channels: Implementation of Countercurrent Operations, Dechema-Infotag-Mikrotrenntechnik: Frankfurt am Main, 2011.
- [13] Jason GK, Sahoo HR, Jensen KF. P. Soc. Photo.-Opt. Ins. 2006, 7, 256-263.
- [14] Scheiff F, Mendorf M, Agar DW, Reis N, Mackley M. P. Soc. Photo.-Opt. Ins. 2011, 11, 1022-1029.
- [15] Aoki, N, Khoo, TH, Okubo, Y, Mae, Proceedings of AIChE, Spring Meeting, April 22-26, 2007, K. Paper No. 89d.
- [16] Barrero A, Loscertales IG. Annu. Rev. Fluid Mech. 2007, 39, 89-106.

- [17] NIST Chemistry WebBook, NIST Standart Reference Database Number 69, National Institute of Standards and Technology: Gaithersburg MD, 2010.
- [18] VDI-Wärmeatlas: Stoffwerte von sonstigen chemisch einheitlichen Flüssigkeiten und Gasen. 10. Auflage, Springer Verlag: Berlin, Heidelberg, 2006.
- [19] Fernandes JB, Scharma MM. Chem. Eng. Sci. 1967, 22, 1267-1282.
- [20] Verma RP, Sharma MM. Chem. Eng. Sci. 1975, 30, 279-292
- [21] Kashid MN, Harsche YM, Agar DW. Ind. Eng. Chem. Res. 2007, 46,8420-8430.
- [22] Kockmann N, Roberge DM. Heat Transfer Eng. 2013, 34,
- [23] Günther A, Khan SA, Thalmann M, Trachsel F, Jensen KF. P. Soc. Photo.-Opt. Ins. 2004, 4, 287-286.
- [24] Jeon W, Shin CB. Chem. Eng. Sci. 2009, 152, 575-582.
- [25] Janovic J, Rebrov EV, Nijhuis TA, Kreutzer MT, Hessel V, Schouten JC. Ind. Eng. Chem. Res. 2012, 51, 1015-1026.
- [26] Mendorf M, Nachtrodt H, Mescher A, Ghaini D, Agar DW. Ind. Eng. Chem. Res. 2010, 49, 10908-10916.
- [27] Kralj JG, Hemantkumar RS, Jensen KF. P. Soc. Photo.-Opt. Ins. 2006, 7, 256-263.



Alexander Holbach studied Biochemical Engineering at TU Dortmund University and finished his degree in 2011 with the diploma thesis "Thermal convection and their stability of a thin rotating liquid drop". In July 2011, he started working as a PhD student at the Laboratory of Equipment Design at TU Dortmund University. The focus of his research is the enantioselective liquid-liquid extraction in process-intensified counter-current contactors.



Norbert Kockmann received his diploma degree in Mechanical Engineering from the Technical University of Munich and received his doctorate in 1996 at the University of Bremen on fouling problems in evaporation. After 5 years in industry, he joined IMTEK at the University of Freiburg in 2001 as group leader of microprocess engineering. In 2007, he finished his habilitation thesis and started at Lonza Ltd., Switzerland. He was responsible for microreactor development and application as well as continuous reaction technology and plant design. In April 2011, Norbert Kockmann was appointed as Bayer Professor at TU Dortmund University and is responsible for equipment design. His research interests are on modular devices, continuous-flow processes and transport phenomena in microstructured devices.